Broere, D. L.J., Mercado, B. Q., Lukens, J. T., Vilbert, A. C., Banerjee, G., Lant, H. M.C., Lee, S. H., Bill, E., Sproules, S. and Holland, P. L. (2018) Reversible ligand-centered reduction in low- coordinate iron formazanate complexes. *Chemistry: A European Journal*, 24(37), pp. 9417-9425.(doi:10.1002/chem.201801298)

Redox-Active Formazanates in Low-Coordinate Iron Chemistry

Daniel L. J. Broere,[,†] Brandon Q. Mercado,[†] James T. Lukens,[‡] Avery C. Vilbert,[‡] Gourab Banerjee,[†] Hannah M. C. Lant,[†] Shin Hee Lee,[†] Eckhard Bill,[§] Stephen Sproules,[⊥] Kyle M. Lancaster,[‡] and Patrick L. Holland*[,†]*

[†]Department of Chemistry, Yale University, New Haven, Connecticut 06520, United States

[‡]Department of Chemistry and Chemical Biology, Baker Laboratory, Cornell University, Ithaca, New York 14853, United States

[§]Max Planck Institute for Chemical Energy Conversion, Stiftstrasse 34-36, D-45470 Mülheim an der Ruhr, Germany

[⊥]WestCHEM, School of Chemistry, University of Glasgow, Glasgow G12 8QQ, United Kingdom

Email: patrick.holland@yale.edu; daniel.broere@yale.edu

Abstract. Coordination of redox-active ligands to metals is a compelling strategy for making reduced complexes more accessible. In this work, we explore the use of redox-active formazanate ligands in low-coordinate iron chemistry. Reduction of an iron(II) precursor occurs at milder potentials than analogous non-redox-active β-diketiminate complexes, and the reduced three-coordinate formazanate-iron compound is characterized in detail. Structural, spectroscopic and computational analysis show that the formazanate ligand undergoes reversible ligand-centered reduction to form a formazanate radical dianion in the reduced species. The less negative reduction potential of the reduced low-coordinate iron formazanate complex leads to distinctive reactivity with formation of a new N-I bond that is not seen with the β-diketiminate analogue. Thus, the storage of an electron on the supporting ligand changes the redox potential and enhances certain reactivity.

Introduction

β-Diketiminate ligands have found extensive use as auxiliary ligands to stabilize unusual metal complexes throughout the periodic table.[1] In particular, highly reduced low-coordinate base metal complexes featuring β-diketiminate ligands are able to activate a number of challenging chemical bonds.[2] Reductive processes in β-diketiminate complexes are normally metal-centered due to the very negative potentials required for ligand-centered reduction.[3] However, the negative potential required for metal-centered reduction (placing electrons in the LUMO at the left of Figure 1) often leads to the use of harsh reductants such as Na or KC_8, which are often incompatible with exogenous substrates for catalytic transformations. Moreover, catalytic turnover is often not feasible because the reduced states are too high in energy.

The ability of redox-active ligands to reversibly accept and donate electrons offers an appealing way to generate more accessible reduced states: as shown on the right of Figure 1, the ligand orbital can be lower in energy, moderating the redox potential. Accessible ligand-centered redox processes can expand upon the intrinsic reactivity of metal centers.[4] Redox-active ligands have enabled multi-electron processes in systems where the transition metal changes oxidation states by less than two electrons, thereby facilitating elementary reactions such as oxidative addition and reductive elimination.[5] Alternatively, redox-active ligands can enable single-electron transformations without changing metal oxidation state.[6] A recent computational investigation by Hu and Chen[7] demonstrated the utility of multiconfigurational calculations for characterizing the redox-active bisiminopyridine ligands, which enable facile reductive elimination in iron-catalyzed [2+2] cycloadditions developed by Chirik and coworkers.[8] Given the wide use of β-diketiminates, there is motivation for exploring a redox-active ligand that is structurally similar, but can readily accept electrons, enabling one-electron reduction at less negative potentials.

Recent studies have shown that β-diketiminates can undergo ligand-centered oxidation in homoleptic complexes of zinc,[9] cobalt,[10] and nickel,[11,12] but isolated transition metal complexes that display ligand-centered reduction have not been reported.[13] Here, we use a formazanate[14] as a redox-active ligand that is structurally similar to β-diketiminates, but which can accept electrons. By placing a low-energy unoccupied ligand orbital near the metal, they could make the complex easier to reduce (Figure 1, right). Otten has shown that formazanates undergo facile ligand-centered reduction when bound to boron and to zinc.[15,16] To our knowledge, reduced formazanates on a redox-active transition metal have not yet been isolated, though they have been spectroscopically observed.[17] Moreover, a recently reported homoleptic formazanate iron(II) complex adopted a low-spin iron(I) configuration upon one-electron reduction rather than generating a ligand-centered radical,[18] highlighting the need for further study.

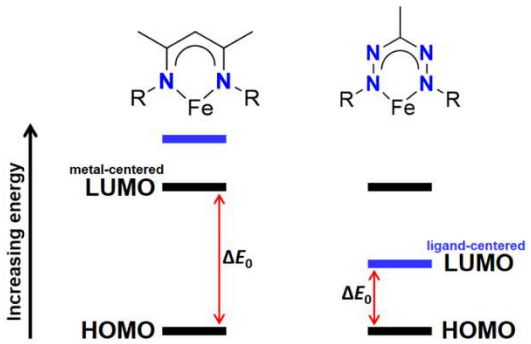

Figure 1. Conceptual representation of how the redox-active formazanate ligand can provide access to a more accessible reduced state.

Herein, we describe the synthesis, characterization and reactivity of some new low-coordinate iron formazanate complexes and their one-electron reduction products. Spectroscopic and computational data are used to characterize the frontier orbitals. These studies reveal that the iron-formazanate complexes undergo ligand-centered reduction at relatively mild potentials, and demonstrate an isolable example of a redox-active metal with a formazanate radical

dianion. In order to illustrate the new opportunities coming from redox activity at the formazanate ligand, we demonstrate how the formazanate complexes activate chemical bonds like low-coordinate β-diketiminate iron complexes, but in contrast the reactions are mediated by ligand-centered redox changes. In addition, we show that the less electron donating formazanate ligand affects the stability of higher metal oxidation states through an unusual N-I elimination reaction.

Results and Discussion

Synthesis and Characterization. The dropwise addition of a suspension of the known[19] formazan **1** to a stirred solution of $Fe[N(SiMe_3)_2]_2$ in pentane gives the three-coordinate formazanate complex **2** in near quantitative yield (Scheme 1). The ^1H NMR spectrum of complex **2** in C_6D_6 at 298 K shows the expected number of paramagnetically shifted resonances between +82 and -40 ppm, which are tentatively assigned based on their relative integration and distance from the metal center (Figure S1). The presence of a single equivalent of THF in the synthesis of complex **2** results in the exclusive formation of the four-coordinate complex **3** (Scheme 1).[20] Hence, care must be taken to avoid the presence of THF in the solvent and starting materials.[21] We observed that the resonance for the $SiMe_3$ protons shifts >40 ppm upfield upon the addition of one equiv of THF to complex **2**. Due to fast exchange on the NMR time scale and an equilibrium constant > 5000 M^{-1}, the chemical shift can be used as an indication of the THF content of the sample (Figure S27).

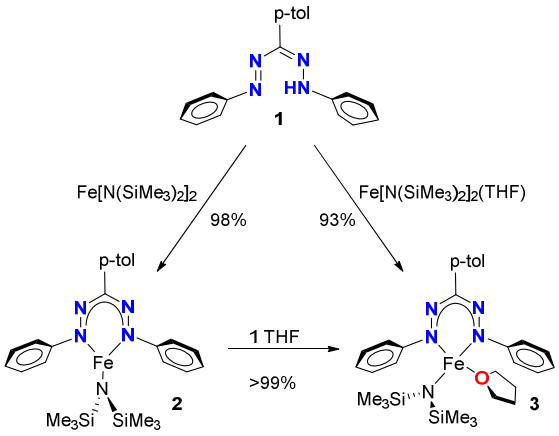

Scheme 1. Synthesis of complexes **2** and **3**

Cooling a solution of **2** or **3** in pentane yielded crystals suitable for single crystal X-ray diffraction. In **2**, two crystallographically independent molecules were found in the asymmetric unit, which share a π–π interaction between the tolyl groups in the formazanate ligands (Figure S37). Each molecule displays a planar, three-coordinate geometry at iron where the sum of the three angles is 359.8 ± 0.5 ° (Figure 2, left). A notable feature in the solid state structure of **2** is the small dihedral angle between the formazanate and N-phenyl groups (1.6 – 28.3°), which is very different from analogous three-coordinate Fe complexes containing a N(SiMe$_3$) and bulky β-diketiminate ligands (65 – 90°).[22] We attribute this difference to the lack of sterically demanding *ortho*-substituents on the *N*-phenyl groups in complex **2**. The Fe–N bond lengths to the formazanates (1.95 – 1.97 Å) are shorter than those in analogous three-coordinate Fe complexes containing a N(SiMe$_3$) and bulky β-diketiminate ligands (1.99 – 2.03 Å).[22] The N–N bond lengths (1.319(5) – 1.327(5) Å) are slightly longer than commonly observed for formazanate complexes (1.30−1.31 Å)[15e,16], which was also observed for the reported homoleptic iron formazanate complex.[18] A notable difference is the significantly longer Fe–N bonds (1.955(4) – 1.966(4) Å) in **2** when compared with the homoleptic bis(formazanate)iron(II) species (1.817(2) − 1.833(2) Å).[18] The solid state structure of complex **3** (Figure 2, right) shows that the iron center adopts a distorted trigonal pyramidal geometry (τ_4

= 0.70 and 0.72)[23] for both molecules in the asymmetric unit. As expected, coordination of an additional ligand causes all Fe–N bond lengths in **3** to be elongated (1.979(2) – 2.000(2) Å) compared to **2**. Interestingly, the bulky amide forces the bound THF into a geometry wherein the C atoms lie over the formazanate ligand.

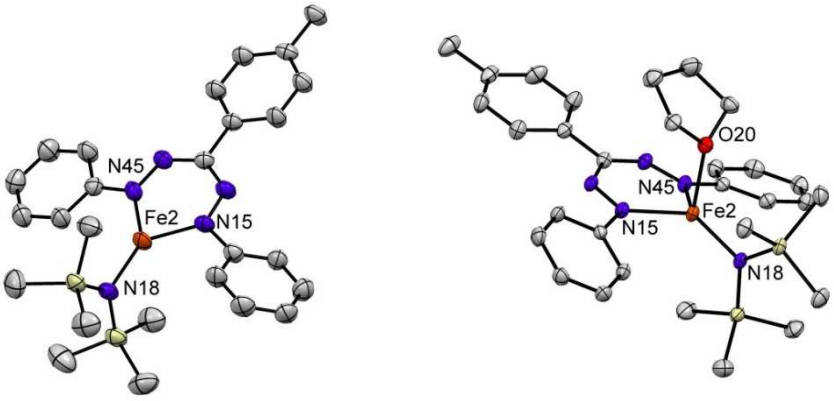

Figure 2. Displacement ellipsoid plots (50% probability) of complex **2** and **3**. Hydrogen atoms have been omitted for clarity. Selected bond lengths (Å) and angles (°) for 2: Fe2–N18 1.903(3); Fe2–N15 1.964(4); Fe2–N45 1.966(4); N18–Fe2–N15 132.5(2); N18–Fe2–N45 135.2(2); N15–Fe2–N45 91.7(1). For 3: Fe2–N18 1.937(2); Fe2–N15 1.979(2); Fe2–N45 1.984(2); Fe2–O20 2.145(1); N18–Fe2–N15 130.40(7); N18–Fe2–N45 127.99(6); N15–Fe2–N45 91.59(6).

Cyclic voltammetry of complex **3** in THF revealed two reversible one-electron reduction events at $E_{½}^{red1}$ = -1.65 V and $E_{½}^{red2}$ = -2.47 V vs Fc^{+}/Fc (Figure S29). The first reduction occurs at a potential ~0.8 V more positive than the corresponding three coordinate β-diketiminate complexes ($E_{½}^{red}$ = -2.4 to -2.6 V vs Fc^{+}/Fc).[24] The nature of this reduction will be discussed below. The addition of $CoCp^*_2$ to a solution of **2** or **3** in hexanes gave the one-electron reduced species **4**, which precipitated as a green solid (Scheme 2). The ^{1}H NMR spectrum of **4** in THF-d_8 at 298 K shows the expected number of paramagnetically shifted resonances between +105 and –25 ppm consistent with a single C_{2v} symmetric species (Figure S9). Intraligand bond

lengths in redox-active ligands can often be used to determine the locus of a redox event.[4-6,16,25] Unfortunately, we were unable to grow crystals of complex **4** that were suitable for X-ray structure determination. Although complex **4** is stable in the solid state for months, it decomposes in THF solution at room temperature within hours to form a mixture of species, concomitant with a color change from dark green to brown. X-ray diffraction of crystals obtained from this mixture afforded a low quality structure revealing a complex wherein the formazanate has undergone N–N bond scission (Figure S39).[26] However, we were unable to isolate sufficient amounts of this unusual product for full characterization, and thus we sought a more stable analogue. Since the C-H bonds in $CoCp^*_2$ and $[CoCp^*_2]^+$ are susceptible to deprotonation or C-H activation,[27] and because of potential stabilizing effects of alkali cations,[28] we used an equivalent of elemental Na to reduce complex **3** in THF, which resulted in a green solution similar in color to **4**. Addition of 2 equiv of 12-crown-4 and cooling the THF mixture gave **5** as a green crystalline solid in 67% yield (Scheme 2). The ^{1}H NMR (Figure S15) and zero-field Mössbauer spectra (vide infra) of **5** are nearly identical to those for complex **4**. However, unlike **4**, complex **5** is stable in solution for days under inert atmosphere. Single crystals suitable for X-ray structure determination were obtained by cooling a THF solution of **5**. The solid state structure reveals that the Na is sandwiched between two crown ethers, and the resulting cation is separated from the anionic formazanate complex (Figure 3). Although the anion in **5** is isostructural to neutral complex **2**, there are some remarkable differences in the bond lengths and angles. The iron amide bond (Fe1–N14) is longer in complex **5** by *ca.* 0.05 Å, suggestive of a more electron-rich Fe center. The N–N bonds within the formazanate are elongated (1.377(6) and 1.345(6) Å) and the Fe–N (formazanate) bonds (1.951(5) and 1.958(5) Å) are shortened compared to **2** (Figure 2), which is consistent with either formazanate-centered reduction or significant π-backdonation into the formazanate ligand.

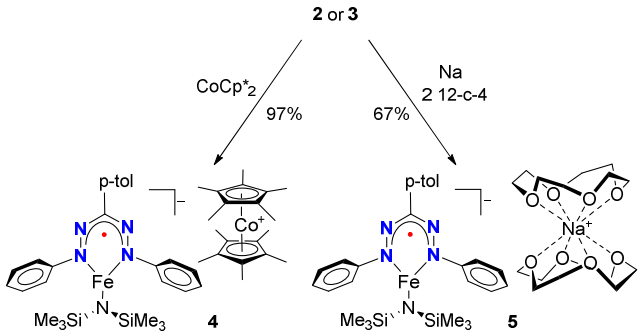

Scheme 2. Synthesis of complexes **4** and **5**

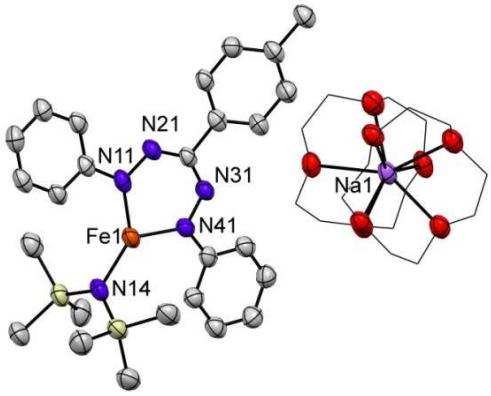

Figure 3. Displacement ellipsoid plot (50% probability) of complex **5**. Hydrogen atoms and a THF molecule have been omitted. Selected bond lengths (Å) and angles (°): Fe1–N11 1.935(5); Fe1–N14 1.951(5); Fe1–N41 1.958(5); N11–N21 1.377(6); N31–N41 1.345(6); N11–Fe1–N14 134.9(2); N11–Fe1–N41 96.5(2); N14–Fe1–N41 128.6(2).

Magnetism and EPR spectroscopy. The temperature dependence of the magnetic susceptibility of solid samples of complexes **2**–**5** was studied in the range 2–290 K using a SQUID magnetometer, and at room temperature in solution using the Evans method. The room temperature magnetic moments of complex **2** and **3** in C_6D_6 solution were 4.8 ± 0.1 μ_B and 4.7 ± 0.1 μ_B, respectively, in agreement with a high-spin iron(II) configuration for both complexes (S = 2, spin-only value $\mu_{s.o.}$ = 4.9 μ_B). In the solid state, three-coordinate **2** and four-coordinate **3** have nearly identical, temperature independent magnetic moments of 5.1 μ_B over the range 30 – 290 K (Figures S4 and S8), which is near the solution values and consistent with a high-

spin iron(II) ($S = 2$) ion in each complex. Below 30 K, the μ_{eff} for **2** decreases under the influence of zero-field splitting. The sign and magnitude of the zero-field parameters were determined from simulations of μ_{eff}(T) in combination with isofield magnetization measurements at 1, 4, and 7 T (Figure S4 inset). Global fitting of the magnetic data yielded $D = -3.8$ cm^{-1} and rhombicity $E/D = 0.19$. The temperature profile is different for **3**, where there is a slight rise in μ_{eff} below 30 K, presumably due to intermolecular interactions. The best fit was obtained for $D = 3.1$ cm^{-1} and $E/D = 0.30$, where the sign of D is opposite to that for three-coordinate **2**, though the sign loses meaning so close to full rhombicity. The similarity in the magnitude of these spin-Hamiltonian parameters for **2** and **3** reveal only a very minor change to the electronic structure upon THF coordination.

Room temperature magnetic moments of 3.8 ± 0.1 μ_B and 3.9 ± 0.1 μ_B were determined from THF solutions of **4** and **5**, respectively, suggesting $S = {}^3/_2$ ground states for both compounds ($\mu_{s.o.} = 3.9\ \mu_B$). Both **4** and **5** exhibited temperature independent effective magnetic moments of 4.0 μ_B over the range 50 – 290 K (Figures S14 and S18), consistent with these values. Much like **2**, **4** shows a low-temperature downturn in μ_{eff} due to zero-field splitting but the more gentle decrease is modelled with a larger $D = -16.8$ cm^{-1} and large rhombicity $E/D = 0.29$. For **5**, on the other hand, the downturn in μ_{eff} is more abrupt, suggesting intermolecular interactions like those observed in **3**. Nevertheless an excellent fit was obtained from modelling the combined μ_{eff}(T) and isofield magnetization plots (including an intermolecular interaction approximation), which gave $D = -10.1$ cm^{-1} and $E/D = 0.26$. These solid state measurements were augmented with an EPR analysis of the odd-electron complexes **4** and **5**. Frozen solution spectra recorded in THF at 10 K highlighted the aforementioned solution instability of **4**. EPR spectra of **4** (Figure S12) show a rhombic $S = {}^3/_2$ signal, and a strong rhombic $S = {}^1/_2$ signal that originates from $[(\text{formazanate})_2\text{Fe}^{\text{I}}]^-$,[18] which is one of the decomposition products of **4** (see SI for more details). The $S = {}^3/_2$ signal has peaks at resonant field positions consistent with an $S =$

$^3/_2$ species having g = (2.17, 2.24, 1.87), D = -5.7 cm^{-1}, and E/D = 0.19 (Figure S12). The greater solution stability displayed by **5** yielded an EPR spectrum (Figure 4) wholly consisting of an S = $^3/_2$ signal with g_{eff} = (2.68, 2.03, 2.34), D = 16 cm^{-1} and E/D = 0.33.

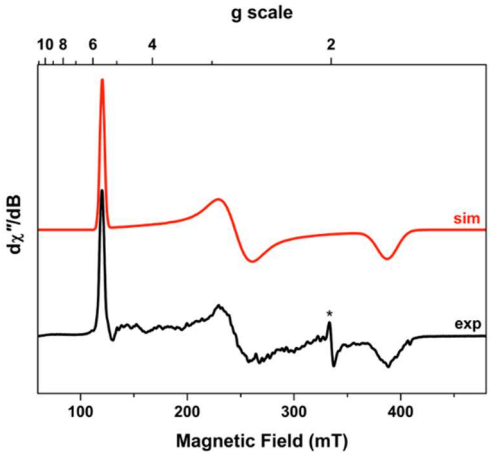

Figure 4. X-band EPR spectrum of **5** in THF at 10 K. Experimental data are represented by the black line; simulation is depicted by the red trace. Asterisk denotes trace impurity contributing <0.5% to the total signal. Experimental conditions: frequency 9.3701 GHz; power 0.2 mW; modulation 2.0 mT.

Minor deviations in g and E/D may be due to structural differences of solid and solution samples (D was taken from magnetic data because the second Kramers doublet could not be determined due to relaxation issues). The increased quality of the S = $^3/_2$ signal in the sample of **5** is consistent with the greater solution stability of this compound. Our assignment of **5** is bolstered by the agreement of g values and zfs parameters between EPR and magnetometry,

Mössbauer spectroscopy. The zero-field Mössbauer spectra of solid samples of **2** and **3** at 80 K (Figure 5) each showed a quadrupole doublet, with **2** at δ = 0.63 mm s^{-1} and $|\Delta E_Q|$ = 2.48 mm s^{-1}, and **3** at δ = 0.71 mm s^{-1} and $|\Delta E_Q|$ = 1.46 mm s^{-1}. These parameters are within the range previously observed for three-[29] and four-coordinate[30] high-spin iron(II) diketiminate

complexes. The smaller quadrupole splitting and larger isomer shift of **3** in comparison to **2** are consistent with the increase in coordination number.[31] The zero-field Mössbauer spectrum of a solid sample of **4** at 80 K shows an asymmetric doublet with δ = 0.48 mm s^{-1} and $|\Delta E_Q|$ = 1.25 mm s^{-1} (Figure 5, bottom), which shows no significant changes upon warming to 173 K. The zero-field Mössbauer spectrum of a solid sample of **5** at 80 K is nearly identical to that of **4,** with δ = 0.49 mm s^{-1} and $|\Delta E_Q|$ = 1.30 mm s^{-1} (Figure S16). The asymmetric broadening of the doublets is common for Kramers systems as a result of intermediate rates of spin relaxation.[32] Interestingly, the change in isomer shift between **2/3** and **4/5** is comparable, but opposite in direction from the reduction of the homoleptic iron formazanate complex reported by Otten and co-workers,[18] which undergoes metal-centered reduction.

Though it is tempting to use the shift in Mössbauer parameters to assign the metal oxidation state, previous results advise caution. In earlier work we described a di(μ-hydrido)diiron(II) complex[33] with a high-spin electronic configuration (S = 2) supported by bulky β-diketiminate ligand that gave a mononuclear three-coordinate iron(I) hydride complex with an S = $^3/_2$ electronic configuration.[34] The change in observed isomer shift in the zero-field Mössbauer spectra of solid samples of the di(μ-hydrido)diiron(II) complex (δ = 0.59 mm s^{-1}) and mononuclear three-coordinate iron(I) hydride (δ = 0.40 mm s^{-1}) at 80 K is comparable to the decrease in isomer shift between **2**/**3** and **4**/**5**. On the other hand, we have also observed similar changes in isomer shift from changes in ligand oxidation state. Namely, oxidation of a four-coordinate high-spin iron(II) complex (S = 2) with a dianionic redox-active tetrazene ligand (δ = 0.81 mm s^{-1}) gives a complex where a tetrazene radical anion (S = $^1/_2$) is strongly antiferromagnetically coupled to a high-spin iron(II) center (S = 2) to give an overall S = $^3/_2$ electronic configuration (δ = 0.69 mm s^{-1}).[35] Consequently, the observed changes in isomer shift between **2**/**3** and **4**/**5** could be attributed to either ligand- or metal-centered reduction.

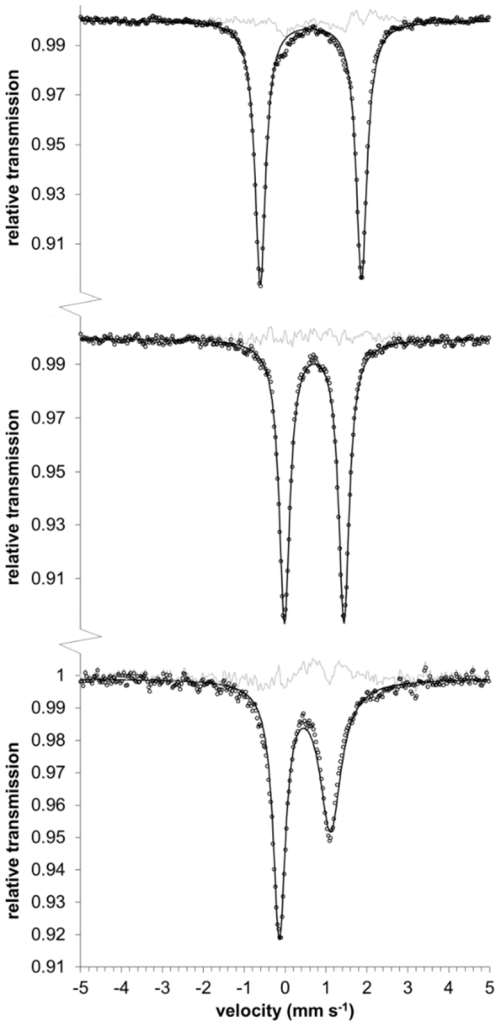

Figure 5. Zero-field Mössbauer spectrum of a solid samples of complex **2** (top), **3** (middle), **4** (bottom) at 80 K. The black circles are experimental data with the fit represented by the black line. The thin grey trace is the residual of the fit.

UV-Vis and X-ray absorption spectroscopy, and computations. The iron(II) complexes **2** and **3** in hexane solution each show an intense absorption in the visible region at 524 nm (19×10^3 cm^{-1}), which we assign as the formazanate $\pi \rightarrow \pi^*$ transition by analogy to intense bands at similar energies uncoordinated formazans.[36] The absorption in these compounds is red-shifted by ca. 30 nm (~1×10^3 cm^{-1}) relative to the protonated formazanate ligand.[15e] In contrast, the electronic spectrum of **5** recorded at in THF at ambient temperature (Figure 6) exhibits prominent absorption bands at 414 and 696 nm ($\varepsilon = 25 \times 10^3$ and 10×10^3 M^{-1} cm^{-1}). Absorption

bands with comparable intensity and position have been observed in reduced triaryl-formazanates bound to redox-inert atoms (carbon:[37] λ = 398 and 721 nm, ε = 7.5 × 10^3 and 3.5 × 10^3 M^{-1} cm^{-1}; boron:[15a] λ = 454 and 716 nm, ε = 15 × 10^3 and 7.5 × $10^3$$M^{-1}$ cm^{-1}; zinc:[15a] λ = 462 and 755 nm, ε = 20 × 10^3 and 10 × 10^3 M^{-1} cm^{-1}), and are diagnostic of a formazanate radical dianion. Together with the Mössbauer and EPR spectrum and magnetism of **5**, the absorption spectrum supports an electronic configuration where a ligand-centered radical (S_L = $^1/_2$) is strongly antiferromagnetically coupled to a high-spin iron(II) center (S_{Fe} = 2) to give an overall S_{total} = $^3/_2$ ground state.

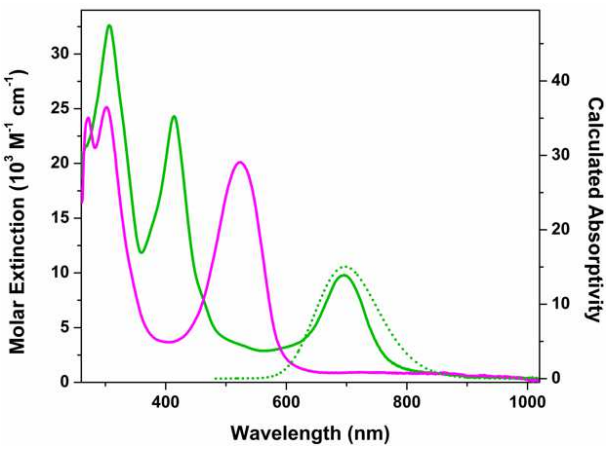

Figure 6. Experimental (solid) and calculated (dotted, SORCI) absorption spectra for complex **3** (pink) and **5** (green) in THF solution.

The Fe K-edge X-ray absorption spectra of **2** – **4** are overlaid in Figure 7. They are characterized by electric dipole forbidden but quadrupole-allowed 1s → 3d pre-edge transitions that appear at the base of the dipole-allowed 1s → *n*p rising edge that dominates a K-edge spectrum. Since the ligand field typically increases with increasing oxidation state for a given ligand set, the pre-edge energy often provides a useful marker for oxidation state. The centers of mass for pre-edge peaks in spectra obtained for **2** – **4** are identical within experimental error at 7112.2 ± 0.1 eV. As a ~1 eV increase in energy is expected per unit of oxidation, the similar edge positions

indicate that the physical Fe oxidation state is the same for the Fe ion in neutral **2** and **3**, and the monoanion in **4**. Moreover, it is noteworthy that the pre-edge peak is of the same intensity for each complex. Electric quadrupole allowed 1s → 3d pre-edge transitions gain intensity through 4p mixing into the 3d orbitals and therefore are sensitive to the symmetry of the complex.[38] Here, the uniform peak height is consistent with the dominant trigonal symmetry in this series where the inclusion of a THF ligand in **3** has little effect on its electronic structure (vide supra). In neutral **2** and **3**, there is a shoulder to higher energy at ~7113.2 eV. In contrast, the shoulder in **4** lies to lower energy at 7111.5 eV, and is tentatively assigned as transition to an orbital with significant ligand character.[39]

Although the rising K-edge is frequently used as an additional metric of physical oxidation state in first-row metals, the rising-edge energies are also influenced by coordination geometry and ligand identity.[40] In the present case, similar edge positions are displayed by three-coordinate **2** and **4** of 7117.0 and 7117.4 eV, respectively, while the edge is shifted by 0.7 eV to higher energy at 7118.1 eV for four-coordinate **3**. Thus, these do not change the conclusion from the pre-edge features, that all the complexes have the same oxidation state at iron.

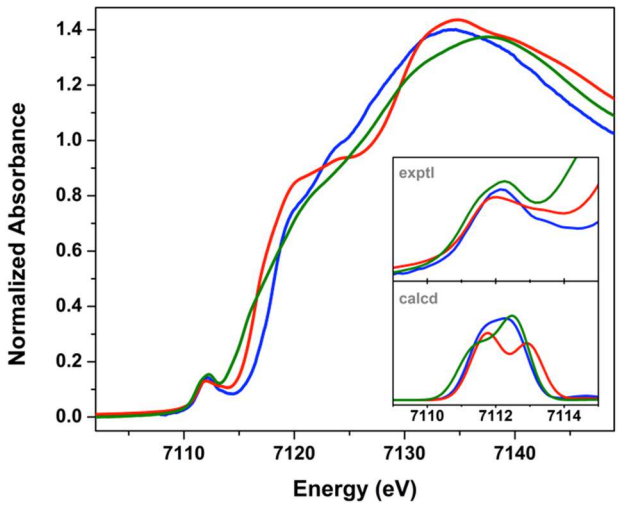

Figure 7. Overlay of the normalized Fe K-edge XAS spectra of **2** (red), **3** (blue), and **4** (green). Inset shows an expansion of the pre-edge region with a comparison of the experimental spectra

above the corresponding calculated spectra obtained from B3LYP TD-DFT calculations. Calculated intensity in arbitrary units.

Density functional theory calculations were carried out to facilitate spectroscopic and electronic structure interpretations. In particular, time-dependent DFT (TDDFT) calculations are known to reproduce metal K-edge XAS with remarkable fidelity after accounting for inaccurate modeling of the 1s core potential with either a scalar or linear energy shift.[41] Time-dependent (TD) DFT calculations (B3LYP hybrid density functional and CP(PPP) basis set on Fe with ZORA-def2-TZVP(-f) on all remaining atoms) were performed on the crystallographic coordinates of each complex. For **2** and **3**, these reproduce the pre-edge region with good fidelity (Fig 7 inset), but the TD-DFT calculation for **4** produces a pre-edge with an energy maximum that is underestimated by 1 eV. Inspection of the frontier orbitals calculated for **4** using this level of theory revealed a straightforward unrestricted Kohn-Sham solution consistent with ($S = {}^{3}/_{2}$) iron(I). Given the consistency of the spectroscopic data described above with an iron(II) configuration, we evaluated a broken-symmetry (BS) option where the four electrons from high-spin iron(II) are allowed to participate in a magnetic interaction with an $S = {}^{1}/_{2}$ formazanate radical anion (BS 4,1). While this approach reproduces the Fe K pre-edge with remarkable fidelity, the BS calculation converges to a *ferromagnetic* $S = {}^{5}/_{2}$ solution, which conflicts with the magnetic measurements. Thus, the single-reference DFT methods fail to acceptably reproduce physical/spectroscopic properties of **4**.

We hypothesized that the ground states of the complex ions in **4** and **5** are multiconfigurational, explaining the poor performance of DFT. Thus, we carried out a multireference configuration interaction (MRCI) calculation using the spectroscopy oriented configuration interaction (SORCI) method.[42] We employed an active space of 11 electrons and 9 orbitals [CAS(11,9)] chosen to include five Fe 3d orbitals and four electrons from the formazanate π system. Five

quartet, doublet, and sextet states were calculated. The chosen active space gave ≥ 90% reference weights for all states. The resulting state energies are given in Table S1. SORCI appropriately predicts a ground-state quartet, with the lowest spin-forbidden excited state–a sextet–occurring at ca. 4000 cm^{-1} to higher energy. The UV-vis absorption spectrum calculated by SORCI reproduces the intense absorption at 14,000 cm^{-1}.

Inspection of the quartet ground state exposes substantial multiconfigurational character. Five configurations have greater than 5% participation in the ground state, with the two leading configurations contributing *ca.* 25% each. Details of these two principal leading configurations are shown in Figure 8. Evaluating the composition of each configuration reveals that the ground state is best described as a nearly equal mix of configurations falling into two electronic structure categories. In one category, high-spin iron(II) participates in antiferromagnetic coupling with the unpaired electron residing in an a_2-symmetry formazanate π^* MO. The second category represents high-spin iron(I) without ligand participation.

In further agreement with our assignment, the homoleptic formazanate iron complex reported by Otten and co-workers,[18] which is proposed to undergo metal-centered reduction, lacks the characteristic absorption bands for ligand-centered reduction that **5** displays at 414 and 696 nm. Overall, the electronic absorption spectra show that the one-electron reduction of the formazanate complexes involves substantial ligand participation.

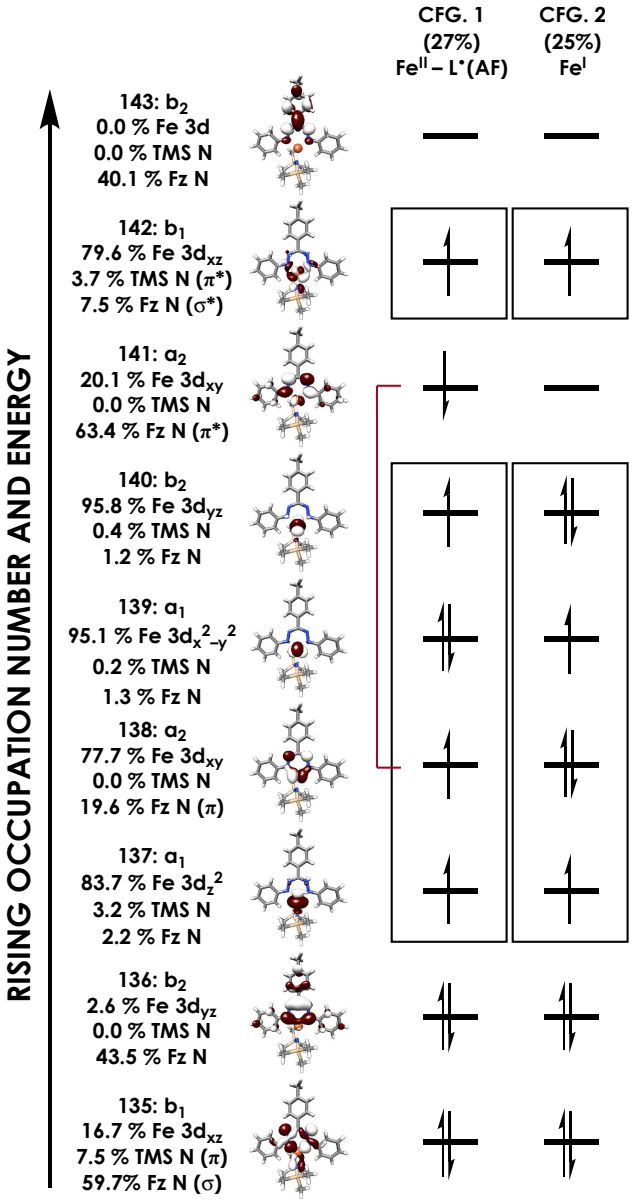

Figure 8. Calculated SORCI averaged atomic natural orbitals (AANOs) comprising the CAS(11,9) reference as well as the two leading configurations comprising the ground-state quartet of the complex ion in **4**. AANOs comprising principally Fe 3d character (the Fe ligand field) are boxed, and the antiferromagnetic (AF) interaction between Fe $3d_{xy}$ and the a_2 formazanate (Fz) π* is indicated with a red bracket. Orbitals are plotted at an isovalue of 0.03 au.

Reactivity of the reduced complexes. No differences are found in the ^{1}H NMR spectra of complexes **4** and **5**, except for resonances attributable to the countercation. Yet, complex **4**

decomposes within hours in solution whereas no signs of decomposition were observed for solutions of **5** over the course of several days (vide supra). To investigate whether this was from reaction between the anion and $CoCp^*_2$ or from sodium stabilization that slows decomposition, $NaBAr^F_4$ was added to a solution of complex **4** and $[CoCp^*_2]PF_6$ was added to a solution of **5**. In both cases decomposition was observed to the same mixture of unidentified species, showing that the decomposition of the one-electron reduced complex is brought about by the presence of the $CoCp^*_2$ cation. Though we have not been able to determine the fate of the $CoCp^*_2$ cation, it is possible that decomposition occurs through a pathway involving C-H activation of one of the Cp* ligands or N-N cleavage in the formazanate.[27]

Reduced low-coordinate β-diketiminate complexes often abstract halide atoms from sp^2 and sp^3 carbon atoms.[43] Considering the significantly less negative reduction potential of **5,** we wanted to evaluate its competence in the activation of C-X (X = halogen bonds). Addition of alkyl and aryl iodides to solutions of **5** results in rapid formation of iron(II) iodide-amide complex **6**, which can also be prepared by reaction of **5** with 0.5 equiv of I_2 or by addition of 1 equiv NaI to solutions of **2** or **3** (Scheme 3). Addition of trityl chloride to a solution of **5** showed formation of triphenylmethyl radical (observed as Gomberg's dimer)[44] and the chloride analogue of **6**.

Accessing the ferric oxidation state was possible by a reaction of **2** or **3** with 0.5 equiv of I_2 giving complex **7**, which has a high-spin iron(III) ($S = {}^5/_2$) configuration (see Supporting Information). Accordingly, we expected that treatment of **5** with one equiv of I_2, or **6** with 0.5 equiv of I_2 in THF, would also give **7**. However, these reactions result in the formation of complex **8**, which still has a high-spin iron(II) ($S = 2$) center, in 82% isolated yield. The only additional reaction product in the oxidations of **5** and **6** is NaI. To test our hypothesis that complex **7** is formed in these reactions but undergoes a decomposition pathway involving NaI we modified the reaction conditions to enable monitoring by ^{1}H NMR spectroscopy. Indeed, the addition of NaI to a THF-d_8 solution of complex **7** gave **8** in 65% spectroscopic yield

together with **6**. Similarly, the addition of I_2 to a THF-d_8 solution of complex **5** gave **8** in 70 % spectroscopic yield together with **6**. In addition, formation of varying amounts of I-N($SiMe_3$)$_2$ and H-N($SiMe_3$)$_2$ were observed in both reactions. The presence of both compounds was confirmed by spiking the mixture with commercial H-N($SiMe_3$)$_2$ and independently synthesized I-N($SiMe_3$)$_2$.[45]

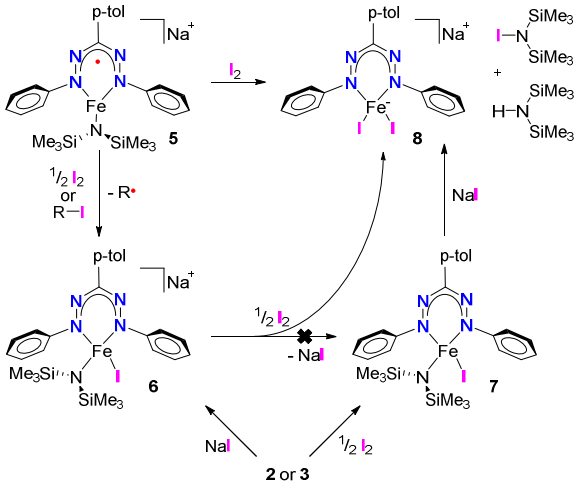

Scheme 3. Reactivity of complex **5** and **7,** and independent synthesis of reaction products.

In the reaction of **7** with NaI an intermediate with very broad resonances is observed, and the apparent concentration is more pronounced at higher NaI concentration. We propose that this intermediate is a five-coordinate Fe(III) species that is formed from **7** and NaI. This five-coordinate species either reductively eliminates I-N($SiMe_3$)$_2$ in analogy to the reaction known for a Ni(IV) complex,[46] or loses •N($SiMe_3$)$_2$[47] as observed for lanthanide complexes.[48] In the latter scenario the formation of I-N($SiMe_3$)$_2$ and H-N($SiMe_3$)$_2$ can be explained by abstraction of an I atom from Fe, and H atom from the THF by •N($SiMe_3$)$_2$, respectively. In the scenario that I-N($SiMe_3$)$_2$ is reductively eliminated from Fe(III), the formation of H-N($SiMe_3$)$_2$ arises from H atom abstraction by •N($SiMe_3$)$_2$, which is formed by reaction of I-N($SiMe_3$)$_2$ with Fe or due its decomposition at room temperature.[45]

In contrast, the β-diketiminate analogue of complex **7** (see Supplementary Information) does not react with stoichiometric or excess NaI. This difference suggests that the formazanate ligand is beneficial for N-I elimination. Both of the potential pathways, reductive elimination and Fe-N homolysis, are thermodynamically more favorable when the lower oxidation state is favored, indicating that the substitution of diketiminate for formazanate successfully modulates the electron density of the iron center in a way that enables new reactivity.

Conclusions

This manuscript has described the synthesis of low-coordinate iron formazanate complexes that can reversibly undergo reduction at a less negative potential compared to analogous iron β-diketiminate species. Distinguishing the high-spin iron(I) description from the antiferromagnetically coupled iron(II)-ligand radical description is challenging, and the distinctive absorption spectra support the latter model. Moreover, multiconfigurational calculations support the presence of a substantial character of iron(II) with a formazanate radical dianion. Thus, in contrast with the earlier reported bis(formazanate) complexes that have predominant iron(I) character,[18] these highly electron-rich amido complexes have electron density on the supporting ligand. To our knowledge, **5** is the first well-characterized complex of a redox-active metal with a formazanate radical dianion. Despite the less negative reduction potential, **5** activates carbon halogen bonds mimicking the reactivity of low valent β-diketiminate iron complexes. In an important difference, the less-electron donating formazanate does not stabilize the higher ferric oxidation state, and therefore a different reaction pathway is followed, leading to N-I elimination.

Acknowledgements. This work was supported by The Netherlands Organization for Scientific Research (Rubicon Postdoctoral Fellowship 680-50-1517 to D.L.J.B.) and the National

Institutes of Health (Grant GM-065313 to P.L.H.). K.M. L. thanks the A. P. Sloan Foundation and the National Science Foundation (CHE-1454455) for funding. P.L.H. thanks the Alexander von Humboldt Foundation for support. We thank Prof. Gary Brudvig for access to an EPR spectrometer.

Keywords: Redox-active ligand • low-coordinate • iron • ligand-centered-radical • formazanate

References

1 a) L, Bourget-Merle, M. F. Lappert, J. R. Severn, *Chem. Rev.* **2002**, *102*, 3031–3066; b) S. Kundu, S. C. E. Stieber, M. G. Ferrier, S. A. Kozimor, J. A. Bertke, T. H. Warren, *Angew. Chem. Int. Ed.* **2016**, *55*, 10321-10325.

2 Selected examples a) K. C. MacLeod, R. A. Lewis, D. E. DeRosha, B. Q. Mercado, P. L. Holland, *Angew. Chem. Int. Ed.* **2017**, *56*, 1069–1072; b) S. Pfirrmann, C. Limberg, C. Herwig, R. Stösser, B. Ziemer, *Angew. Chem. Int. Ed.* **2009**, *48*, 3357–3361; c) T. R. Dugan, E. Bill, K. C. MacLeod, G. J. Christian, R. E. Cowley, W. W. Brennessel, S. Ye, F. Neese, P. L. Holland, *J. Am. Chem. Soc*. **2012**, *134*, 20352–20364; d) B. Horn, C. Limberg, C. Herwig, B. Braun, *Chem. Commun.* **2013**, *49*, 10923; e) X. Dai, P. Kapoor, T. H. Warren, *J. Am. Chem. Soc.* **2004**, *126*, 4798–4799.

3 For exceptions see: a) O. Eisenstein, P. B. Hitchcock, A. V. Khvostov, M. F. Lappert, L. Maron, L. Perrin, A. V. Protchenko, *J. Am. Chem. Soc.*, **2003**, *125*, 10790–10791. b) A. G. Avent, P. B. Hitchcock, A. V. Khvostov, M. F. Lappert, A. V. Protchenko, *Dalton Trans.* **2004**, *33*, 2272–2280.

4 a) D. L. J. Broere, R. Plessius, J. I. van der Vlugt, *Chem. Soc. Rev.* **2015** 44, 6886–6915; b) O. R. Luca, R. H. Crabtree, *Chem. Soc. Rev.* **2013**, 42, 1440–1459; c) V. K. K. Praneeth, M. R.

Ringenberg, T. R. Ward, *Angew. Chem. Int. Ed.* **2012**, 51, 10228–10234; d) J. I. van der Vlugt, *Eur. J. Inorg. Chem.* **2012**, 363–375; e) V. Lyaskovskyy, V.; B. de Bruin, *ACS Catal.* **2012**, *2*, 270–279; f) W. Kaim, *Inorg. Chem.* **2011**, 50, 9752–9765; g) P. J. Chirik, K. Wieghardt, *Science* **2010**, 327, 794–795.

5 a) S. A. Johnson, R. F. Higgins, M. M. Abu-Omar, M. P. Shores, S. C. Bart, *Organometallics* **2017**, *36*, 3491−3497; b) J. L. Wong, R. H. Hernández Sánchez, J. Glancy Logan, R. A. Zarkesh, J. W. Ziller, A. F. Heyduk, *Chem. Sci.* **2013**, *4*, 1906-1910; c) S. J. Kraft, P. E. Fanwick, S. C. Bart, *J. Am. Chem. Soc.* **2012**, *134*, 6160-6168; d) M. R. Haneline, A. F. Heyduk *J. Am. Chem. Soc.* **2006**, *128*, 8410-8411.

6 a) J. Jacquet, K. Cheaib, Y. Ren, H. Vezin, M. Orio, S. Blanchard, L. Fensterbank, M. Desage-El Murr *Chem. Eur. J.* **2017**, *23*,15030 –15034; b) D. Fujita, H. Sugimoto, Y. Shiota, Y. Morimoto, K. Yoshizawa, S. Itoh, *Chem. Commun.* **2017**, *53*, 4849-4852; c) J. Jacquet, S. Blanchard, E. Derat, M. Desage-El Murr, L. Fensterbank, *Chem. Sci.* **2016**, *7*, 2030-2036; d) D. L. J. Broere, D. K. Modder, E. Blokker, M. A. Siegler, J. I. van der Vlugt, *Angew. Chem. Int. Ed.* **2016**, *55*, 2406-2410; e) D. L. J. Broere, B. de Bruin, J. N. H. Reek, M. Lutz, S. Dechert, J. I. van der Vlugt, *J. Am. Chem. Soc.* **2014**, *136*, 11574-11577.

7 L. Hu, H. Chen, *J. Am. Chem. Soc.* **2017**, *139*, 15564-15567.

8 a) J. M. Hoyt, V. A. Schmidt, A. M. Tondreau, P. J. Chirik, *Science* **2015**, *349*, 960-963; b) M. W. Bouwkamp, A. C. Bowman, E. Lobkovsky, P. J. Chirik, *J. Am. Chem. Soc.* **2006**, *128*, 13340-13341; c) J. M. Hoyt, K. T. Sylvester, S. P. Semproni, P. J. Chirik, *J. Am. Chem. Soc.* **2013**, *135*, 4862-4877; d) S. K. Russell, E. Lobkovsky, P. J. Chirik, *J. Am. Chem. Soc.* **2011**, *133*, 8858-8861.

9 M. M. Khusniyarov, E. Bill, T. Weyhermüller, E. Bothe, K. Wieghardt, *Angew. Chem., Int. Ed.* **2011**, *50*, 1652–1655.

10 M. P. Marshak, M. B. Chambers, D. G. Nocera, *Inorg. Chem.* **2012**, *51*, 11190–11197.

11 J. Takaichi, Y. Morimoto, K. Ohkubo, C. Shimokawa, T. Hojo, S. Mori, H. Asahara, H. Sugimoto, N. Fujieda, N. Nishiwaki, S. Fukuzumi, S. Itoh, *Inorg. Chem.*, **2014**, *53*, 6159–6169.

12 For a review on the non-innocence of β-diketiminate ligands see: C. Camp, J. Arnold, *Dalton Trans.* **2016**, *45*, 14462-14498.

13 Recent work using fluorinated β-diketiminates on Pt suggests suggests that ligand-centered reduction could be feasible: K. S. Choung, M. D. Islam, R. W. Guo, T. S. Teets, *Inorg. Chem.* **2017**, *56*, 14326−14334.

14 a) J. B. Gilroy, P. O. Otieno, M. J. Ferguson, R. McDonald, R. G. Hicks, *Inorg. Chem.*, **2008**, *47*, 1279–1286; b) A. W. Nineham, *Chem. Rev.*, **1955**, *55*, 355–483.

15 a) M. –C. Chang, E. Otten, *Chem. Commun.* **2014**, *50*, 7431–7433; b) M.–C. Chang, A. Chantzis, D. Jacquemin, E. Otten, *Dalton Trans*. **2016**, *45*, 9477–9484; c) S. M. Barbon, J. T. Price, P. A. Reinkeluers, J. B. Gilroy, *Inorg. Chem.* **2014**, *53*, 10585−10593; d) R. Mondol, D. A. Snoeken, M. –C. Chang, E. Otten, *Chem. Commun.* **2017**, *53*, 513−516; e) J. B. Gilroy, M. J. Ferguson, R. McDonald, B. O. Patrick, R. G. Hicks, *Chem. Commun*. **2007**, 126–128.

16 a) M. –C. Chang, T. Dann, D. P. Day, M. Lutz, G. Wildgoose, E. Otten, E. *Angew. Chem. Int. Ed.* **2014**, *53*, 4118 –4122; b) M. –C. Chang, P. Roewen, R. Travieso-Puente, M. Lutz, E. Otten, *Inorg. Chem.* **2015**, *54*, 379−388.

17 a) A. Mandal, B. Schwederski, J. Fiedler, W. Kaim, G. K. Lahiri, *Inorg. Chem.* **2015**, *54*, 8126−8135; b) E. Kabir, C. –H. Wu, J. I. Wu, T. S. Teets, *Inorg. Chem.* **2016**, *55*, 956−963; c) J. B. Gilroy, B. O. Patrick, R. McDonald, R. G. Hicks, *Inorg. Chem.* **2008**, *47*, 1287−1294; d) S. Hong, L. M. R. Hill, A. K. Gupta, B. D. Naab, J. B. Gilroy, R. G. Hicks, C. J. Cramer, W. B. Tolman, *Inorg. Chem.* **2009**, *48*, 4514−4523.

18 R. Travieso-Puente, J. O. P. Broekman, M. –C. Chang, S. Demeshko, F. Meyer, E. Otten, *J. Am. Chem. Soc.* **2016**, *138*, 5503−5506.

19 J. B. Gilroy, M. J. Ferguson, R. McDonald, B. O. Patrick, R. G. Hicks, *Chem. Commun.* **2007**,126-128.

20 For the difference in reactivity between **2** and **3** see: D. L. J. Broere, B. Q. Mercado, P. L. Holland, *Angew. Chem. Int. Ed.* **2018**, in press, DOI: 10.1002/anie.201802357.

21 D. L. J. Broere, I. Čorić, A. Brosnahan, P. L. H. Holland, *Inorg. Chem.* **2017**, *56*, 3140–3143.

22 A. Panda, M. Stender, R. J. Wright, M. M. Olmstead, P. Klavins, P. P. Power, *Inorg. Chem.* **2002**, *41*, 3909–3916.

23 L. Yang, D. R. Powell, R. P. Houser, *Dalton Trans.* **2007**, 955–964.

24 K. P. Chiang, P. M. Barrett, F. Ding, J. M. Smith, S. Kingsley, W. W. Brennessel, M. M. Clark, R. J. Lachicotte, P. L. Holland, *Inorg. Chem.* **2009**, *48*, 5106–5116.

25 a) S. N. Brown, *Inorg. Chem.* **2012**, *51*, 1251−1260; b) D. L. J. Broere, R. Plessius, J. Tory, S. Demeshko, B. de Bruin, M. A. Siegler, F. Hartl, J. I. van der Vlugt, *Chem. Eur. J.* **2016**, *22*, 13965−13975; c) D. L. J. Broere, N. P. van Leest, M. A. Siegler, J. I. van der Vlugt, *Inorg. Chem.* **2016**, *55*, 8603−8611; d) S. Sproules, K. Wieghardt, *Coord. Chem.Rev.* **2010**, *254*, 1358-1382.

26 The N-N bond scission is possibly facilitated by isomerization of the reduced formazanate from a 6- to 5-membered chelate: D. L. J. Broere, B. Q. Mercado, E. Bill, K. M. Lancaster, S. Sproules, P. L. Holland, *Inorg. Chem.* **2018**, in press, DOI: 10.1021/acs.inorgchem.8b00226

27 a) K. C. MacLeod, S. F. McWilliams, B. Q. Mercado, P. L. Holland, *Chem. Sci.* **2016**, *7*, 5736-5746; b) Y. Ohki, A. Murata, M. Imada, K. Tatsumi, *Inorg. Chem.* **2009**, *48*, 4271-4273.

28 a) K. C. MacLeod, F. S. Menges, S. F. McWilliams, S. M. Craig, B. Q. Mercado, M. A. Johnson, P. L. Holland, *J. Am. Chem. Soc.* **2016**, *138*, 11185−11191; b) S. F. McWilliams, K. R. Rodgers, G. Lukat-Rodgers, B. Q. Mercado, K. Grubel, P. L. Holland, *Inorg. Chem.* **2016**, *55*, 2960−2968; c) K. Grubel, W. W. Brennessel, B. Q. Mercado, P. L. Holland, *J. Am. Chem. Soc.* **2014**, *136*, 16807−16816; d) G. P. Connor, P. L. Holland, *Catalysis Today* **2017**, *286*, 21−40.

29 S. F. McWilliams, E. Brennan-Wydra, K. C. MacLeod, P. L. Holland, *ACS Omega* **2017**, *2*, 2594−2606.

30 a) N. A. Arnet, T. R. Dugan, F. S Menges, B. Q. Mercado, W. W. Brennessel, E. Bill, M. A. Johnson, P. L. Holland, *J. Am. Chem. Soc.* **2015**, *137*, 13220-13223; b) R. A. Lewis, K. C. MacLeod, B. Q. Mercado, P. L. Holland, *Chem. Commun.* **2014**, *50*, 11114-11117.

31 a) C. Kleinlein, A. J. Bendelsmith, S. –L. Zheng, T. A. Betley, *Angew.Chem. Int.Ed.* **2017**, *56*, 12197-12201; b) J. J. Dunsford, D. J. Evans, T. Pugh, S. N. Sha, N. F. Chilton, M. J. Ingleson,

Organometallics **2016**, *35*, 1098−1106; c) D. J. Evans, D. L. Hughes, J. Silver, *Inorg. Chem.* **1997**, *36*, 747-748.

32 P. Gülich, E. Bill, A. X. Trautwein, *Mössbauer Spectroscopy and Transition Metal Chemistry*, Springer, Heidelberg, 2011.

33 Initial synthesis: J. M. Smith, R. J. Lachiocotte, P. L. Holland, *J. Am. Chem. Soc.* **2003**, *125*, 15752-15753; Mössbauer spectrum and alternative synthesis: T. R. Dugan, P. L. Holland, *J. Organomet. Chem.* **2009**, *694*, 2825-2830.

34 K. P. Chiang, C. C. Scarborough, M. Horitani, N. S. Lees, K. Ding, T. R. Dugan, W. W. Brennessel, E. Bill, B. M. Hoffman, P. L. Holland, *Angew. Chem. Int. Ed.* **2012**, *51*, 3658-3662.

35 R. E. Cowley, E. Bill, F. Neese, W. W. Brenessel, P. L. Holland, *Inorg. Chem.* **2009**, *48*, 4828-4836.

36 a) H. Tezcan, S. Can, R. Tezcan, *Dyes Pigm.* **2002**, *52*, 121; b) Y. A. Ibrahim, A. A. Abbas, A. H. M. J. Elwaby, *Heterocycl. Chem.* **2004**, *41*, 135.

37 J. B. Gilroy, S. D. J. McKinnon, B. D. Koivisto, R. G. Hicks, *Org. Lett.* **2007**, *9*, 4837−4840.

38 R. G. Shulman, Y. Yafet, P. Eisenberger, W. E. Blumberg, *Proc. Natl. Acad. Sci. U.S.A.* **1976**, *73*, 1384–1388.

39 P. Banerjee, S. Sproules, T. Weyhermüller, S. DeBeer George, K. Wieghardt, *Inorg. Chem.*, **2009**, *48*, 5829–5847.

40 a) S. N. MacMillan, K. M. Lancaster, *ACS Catal.* **2017**, *7*, 1776−1791; b) L. S. Kau, D. J. Spira-Solomon, J. E. Penner-Hahn, K. O. Hodgson, E. I. Solomon, *J. Am. Chem. Soc.* **1987**, *109*, 6433–6442.

41 S. DeBeer George, T. Petrenko, F. Neese, *J. Phys. Chem. A* **2008**, *112*, 12936–12943.

42 F. Neese, *J. Chem. Phys.* **2003**, *119*, 9428.

43 Selected examples: a) T. R. Dugan, J. M. Goldberg, W. W. Brennessel, P. L. Holland, *Organometallics* **2012**, *31*, 1349−1360; b) T. R. Dugan, X. Sun, E. V. Rybak-Akimova, O. Olatunji-Ojo, T. R. Cundari, P. L. Holland, *J. Am. Chem. Soc.* **2011**, *133*, 12418–12421; c) W. Zhou, L. Tang, B. O. Patrick, K. M. Smith, *Organometallics*, **2011**, *30*, 603–610; d) J. M. Smith, A. R. Sadique, T. R. Cundari, K. R. Rodgers, G. Lukat-Rodgers, R. J. Lachiotte, C. J.

Flachenriem, J. Vela, P. L. Holland, *J. Am. Chem. Soc.*, **2006**, *128*, 756–769; e) J. C. Doherty, K. H. D. Ballem, B. O. Patrick, K. M. Smith *Organometallics* **2004**, *23*, 1487-1489.

44 H. Lankamp, W. T. Nauta, C. MacLean, *Tet. Lett.* **1968**, *9*, 249-254.

45 R. E. Bailey, R. West, *J. Organomet. Chem.* **1965**, *4*, 430−439.

46 J. J. Laarhoven, P. Mulder, *J. Phys. Chem. B* **1997**, *101*, 73−77.

47 M. D. Cook, B. P. Roberts, K. Singh, ***J. Chem. Soc., Perkin Trans. 2***, **1983**, 635−643.

48 a) A. J. Lewis, P. J. Carroll, E. J. Schelter, *J. Am. Chem. Soc.* **2013**, *135*, 511−518; b) K. C. Mullane, A. J. Lewis, H. Yin, P. J. Carroll, E. J. Schelter, *Inorg. Chem.* **2014**, *53*, 9129−9139.